*Materials and Manufacturing Processes*, 23: 823–828, 2008

ISSN: 1042-6914 print/1532-2475 online
DOI: 10.1080/10426910802384672

Taylor & Francis
Taylor & Francis Group

# Thermal and Structural Characterization of Copper–Steel Bonding Interfaces Produced by Impact Welding

Ignacio Rojas-Rodriguez[1,2], D. Jaramillo-Vigueras[1], R. Velázquez-Hernández[4], A. Del Real[3], I. Serroukh[4], L. Baños[5], J. García[6], and M. E. Rodríguez-García[3,4]

[1]*Centro de Investigación e Innovación Tecnológica del Instituto Politécnico Nacional, Santa Catarina, México*
[2]*Departamento de Procesos de Producción, Universidad Tecnológica de Querétaro, Querétaro, Qro. México*
[3]*Departamento de Nanotecnología, Centro de Física Aplicada y Tecnología Avanzada, Universidad Nacional Autónoma de México, Querétaro, Qro. México*
[4]*Facultad de Ingeniería, Postgrado en Ingeniería, Universidad Autónoma de Querétaro, Querétaro, Qro. México*
[5]*Instituto de Investigación en Materiales, Universidad Nacional Autónoma de México, México D.F., México*
[6]*Photothermal Diagnostic Inc., Toronto, Ontario, Canada*

A complete characterization of Cu–steel impact welded were made using photothermal radiometric (PTR) spectroscopy, scanning electron microscopy (SEM), microhardness, and X-ray diffraction (XRD) in order to study the changes in the structural, metallurgical, and thermal properties of Impact Welding Zone (IWZ) and the Impact Affected Zone (IAZ) after the impact welding. Three samples with different morphological interfaces were prepared for this analysis. According to the SEM analysis in etched samples, it was possible to determine that the IWZ is formed by the collapse of grains of Cu and steel (ferrite and pearlite) into the Cu–steel interface and the IAZ are formed in a region close to the IWZ with low grain damage. Microhardness Vickers test is able to detect the IAZ in all cases, but due to its contact character, it is not possible to obtain continuous hardness information across the Cu–steel interface. According to the XRD patterns after the impact welding process, no new phase was formed. Noncontact PTR amplitude and phase images are able to identify the IAZ and the IWZ.

*Keywords* Crystallinity; Cu–steel bonding; Ferrite; Heat; Impact affected zone; Impact welding; Impact welding zone; Interface; Noncontact; Perlite; Photothermal characteization; Structural properties; Thermal diffusivity; Thermal properties; Thermal wave; Vickers hardness.

## 1. Introduction

Impact welding is a technique to joining metals with different physical and metallurgical properties, like low-melting metals and alloys with dissimilar metals such as steel and copper [1] because it is not possible to weld these metals using conventional technique (arc welding) [2]. The process occurs extremely fast, unlike conventional welding processes, although the parameters have been established for most metal combinations by using destructive methods such as: tensile, metallographic analysis, impact, and shear tests [3]. The phase formation in the Fe–Cu system has been extensively investigated [4]. The nondestructive methods to characterize the welding unions are an impetus today; PTR technique [5] is ideal for this purpose: it is based in the measurement of modulated thermal infrared radiation emitted from a selected area after absorption of modulated laser radiation. Velazquez et al. [6] used photothermal images to study the Te distribution on 2 inches GaSb wafer, and determine that the Te was segregated toward the wafer's edge. Garcia et al. [5, 7] characterized thermophysical properties of thermal sprayed coatings on carbon steel. In the case of metals, the PTR signals are from the thermal processes which are affected by the thermal properties [8]. X-ray diffraction (XRD) is an excellent tool to study the structural transformation in welding process. Recently, Rangel-Ortiz et al. [9] used the changes in the full width half maximum (FWHM ) of XRD patterns of $\alpha$-Al to investigate the presence of Lithium and Hf in Al alloys as-cast. They found that the presence of Li can be determined by reduction in the lattice parameter measures in the (111) direction as well as the changes in the crystalline quality stated by the changes of the FWMH. Curiel et al. [2] used XRD, and the FWHM variations on the heat-affected zone for steel cooled with different quenchants, water, oil, and air. Yu Liu et al. [10] used photothermal radiometric (PTR) phase image on heat-treated case hardened steels to study the hardness profiles.

The main objective of this article is to show the ability of PTR to study the interface of Cu–steel after the impact welding. The PTR images on bonding zone were used to analyze the thermal changes at the interface. Also, XRD analysis of each peak of copper and steel were used to characterize the structural changes produced by the impact process at the interface. The changes of the FWHM for each peak as well as the peaks shift allow for evaluation of the crystalline quality of Cu and steel after the welding process.

## 2. Experimental setup and methodology

### 2.1. Sample Description

Samples (A, B, and C) were prepared from a commercial copper plate with 99.9% purity and plain carbon steel plates

Received February 7, 2008; Accepted May 22, 2008
Address correspondence to M. E. Rodríguez-García, Departamento de Nanotecnología, Centro de Física Aplicada y Tecnología Avanzada, Universidad Nacional Autónoma de México, Campus Juriquilla, Apartado Postal, 1-1010. C.P. 76230, Querétaro Qro. México; E-mail: marioga@fata.unam.mx

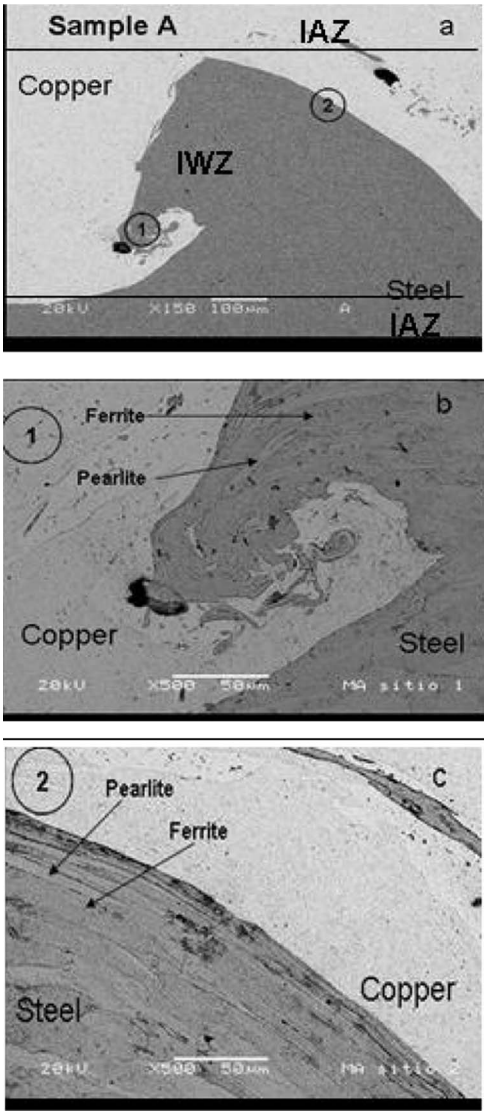


FIGURE 1.—(a) (150X); (b) (500X); and (c) (500X) show sample A at the IWZ produced by the impact and the deformation on points 1 and 2.

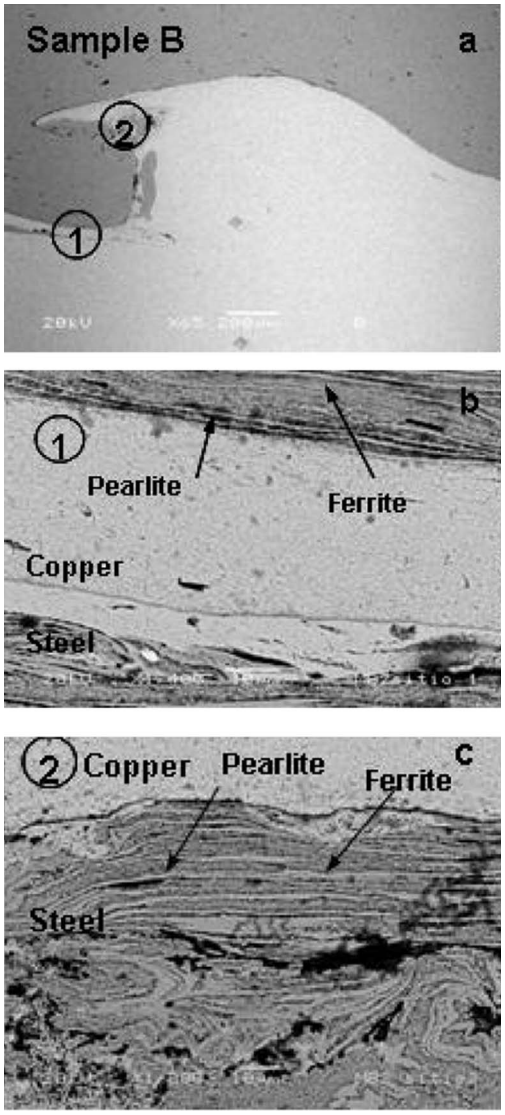


FIGURE 2.—(a) (100X); (b) (1000X); and (c) (2000X) show the sample B on the IWZ and the deformation on points 1 and 2, produced by the impact.

(AISI-SAE 1020) that were 4 inches in diameter and 0.5 thick. The samples were made with different interfaces shapes (samples A and B by machining), before impact bonding. The velocity of impact for samples A and B was 627 m/s with an impact angle of 20° and, 513 m/s and 20° impact angle for sample C. The equipment used was a cannon pressurized with air. The blank was the steel plate and the projectile was copper. Figure 1(a) shows (sample A) the scanning electron microscopy (SEM) images of Cu–steel with small wave teeth, with 45° intersect surface (between root teeth and top teeth), 1 mm wide and 1 mm high. Figure 2(a) shows the SEM images of sample B. Finally, Fig. 3(a) shows the SEM images of the welding between Cu–steel with smooth interface (sample C). In these figures, the region close to the interface welding is called Impact Welding Zone (IWZ); in this zone, the metal had been deformed directly by the impact, and major deformation in the structure occurs. The region beside the IWZ is called Impact Affected Zone (IAZ), where there is less structural deformation.

### 2.2. SEM

The metallographic analyses of the polished (alumina 0.3 μm) samples were done using a SEM system, Philips XL-30, at high vacuum. The samples were etched with nital 2% for steel and ammonium persulfate for Cu.

### 2.3. PTR and Experimental Setup

In PTR, the resulting of periodic heat flow in the material due to the absorption of light on a surface sample is a diffusive process that produces a temperature distribution known as thermal wave. PTR was used for characterizing impact bonding between copper and steel metals with different thermal properties (thermal diffusivity and conductivity); this leads to differences in the measured

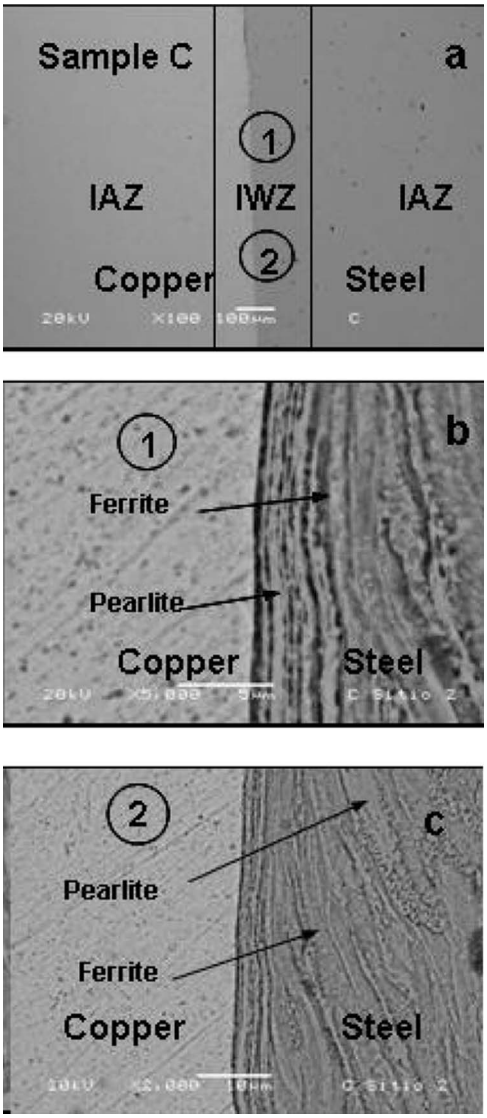


FIGURE 3.—(a) (100X); (b) (5000X); and (c) (2000X) show the sample C on the IWZ produced by the impact and the deformation on points 1 and 2.

amplitude and phase, allowing the thermal mapping of the interface. The schematic experimental setup and description of the system and theory has been presented elsewhere [7, 11]. A modulate diode laser with a spot size of 40 μm (25 mW on the sample) is focused on the sample. The sample is mounted on an X–Y translation stage driven by stepping motors. Image scans were made at fixed frequency (10 KHz), and at this frequency the PTR amplitude and phase signals exhibit changes on the surfaces [7]. The IR emission from the sample is collected by collimating off-axis mirrors and focused onto a cooled HgCdTe detector (2–12 μm). The PTR amplitude and phase signals were fed into a lock-in amplifier, a PC was used to store the experimental data.

*2.3.1. Pothermal Images.* The thermal image of sample A was obtained by scanning a 3 mm × 3 mm area. The images were formed on 50 lines with 50 points per line, with 60 μm separations between the points and lines. Sample B was a scan a 10 mm × 10 mm area, the lines and points separation was 100 μm. Finally, the explored area of sample C was the same as that for sample A with 50 lines and 50 points per line. The separation distance between neighboring points was 50 μm [6, 7, 11].

### *2.4. XRD Measurement*

The structural changes in the IAZ and IWZ were studied (6 mm × 6 mm). The XRD patterns (30 to 120°, $2\theta$ scale) were taken using a Siemens Crystaloflex 5000 operating at 35 kV, 15 mA with Cu $K_\alpha$ line. The experimental FWHM was analyzed using a Dataflex program. The X-ray patterns were used to study the crystalline phases and also the shift of the characteristic peaks of Cu–steel due to the interface impact junction [2, 9].

### *2.5. Microhardness Vickers*

The Vickers microhardness test was done on the IAZ and IWZ on polished samples (alumina 0.3 μm) using 500 grams load to show the hardness profile variation along Cu and steel after impact welding. Microhardness Tester Leco Model LM300AT was used. Images from 100 hardness values per sample over 10 lines perpendicular to the interface separated 1 mm width gaps were obtained with 10 hardness values per line across the interface each point having a separation of 500 μm. This separation is based on the fact that microhardness is a destructive test and the approximation between consecutive test points can affect the structure, causing erroneous values will occur.

## 3. RESULTS

### *3.1. SEM Analysis*

Figure 1(a) shows the image of one tooth of Cu–steel located in the IWZ of sample A (without etching) for points 1 and 2. Figure 1(b) (etched) shows, the top teeth area and the IWZ, where the major deformation in the metallurgical microstructure and high stress occurs. No fissures at the Cu–steel interface were detected. Figure 1(c) reveals the deformation of pearlite and ferrite located at the IWZ. Figure 2 shows the SEM images of sample B and a tooth at the IWZ, for two points. In Fig. 2(b), the root tooth area at the IWZ (point 1) is shown. Here, notice the deformation produced by the impact. Figure 2(c) presents the area deformed at the top tooth due to the impact and the high deformation of pearlite and ferrite. Figure 3 (sample C) shows similar results to those in samples A and B, the difference being the finished smooth surface, and the IWZ is minor, which is clearly demonstrated in Fig. 3(b) and (c).

Considering the aforementioned results, the IWZ depends on the impact area; if the impact area of Cu and Steel increases, the IWZ also increases. On the other hand, the IAZ decreases if the impact area decreases. Based on these observations, it is possible to define the IWZ as the region where high grain Cu–steel plastic deformations exist, and IAZ as the region where grain deformations is lower.

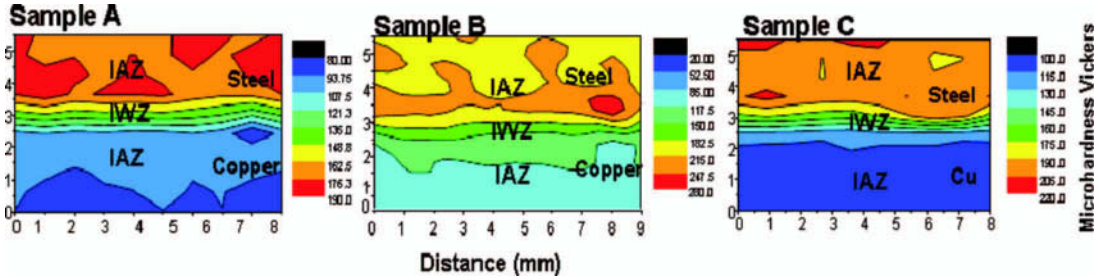


FIGURE 4.—Microhardness profile on all three samples A, B, and C, on IAZ.

### 3.2. Microhardness

The Vickers microhardness test was done on the IAZ crossing the interface (IWZ) of the three samples. The profile of microhardness is shown in Fig. 4. The microhardness in all samples increment at the IWZ and in the IAZ as a result of the impact.

### 3.3. PTR

The thermal wave generated at the sample surface by the absorption of laser radiation becomes attenuated at a distance of $\mu$. This was the only information available due to changes in the thermal properties of the sample surface. The thermal diffusivity of Cu is $\alpha = 1.17\,\mathrm{cm}^2/\mathrm{s}$ has a thermal length defined by [8] $\mu = \sqrt{\frac{\alpha}{\pi f}}$, where $f = \omega/2\pi$ is the frequency and $\omega$ the angular frequency, while for steel, $\alpha = 0.227\,\mathrm{cm}^2\,\mathrm{seg}^{-1}$ [12]. Figures 5(a)–(f) show the PTR thermal images in amplitude and the phase obtained from samples A, B, and C, respectively. The higher PTR signal amplitude values belong to the steel and the lowest ones correspond to Cu. The higher PTR signal phase values in this case belong to Cu and the lower ones to steel. As the samples have the same surface finish the reflection coefficient for 532 nm are different, according to Figs. 5(a), (c), and (d), the radiation to heat conversion in steel is greater than in Cu. Therefore, the PTR amplitude signal in the case of steel is bigger. In the case of sample A, the steel close to the interface, PTR amplitude signal decreases can be observed. This is not a sharp boundary [Fig. 5(a)]. In the case of sample B, this effect is less, while in sample C there is not phase mixing. A sharper PTR amplitude boundary can also be observed. The length of the thermal diffusion and therefore the thermal diffusivity determine the damping of the thermal wave as well as the phase lag between the excitation and the thermal response of the system. Consequently, the measured PTR amplitude signal is proportional to the reciprocal of the thermal effusivity, while the PTR phase lag will be proportional to the $x/\mu$ term. The thermal effusivity of Cu is greater than that of steel. The amplitude of the thermal wave in Cu will be lower than that steel surface, as indicated by the amplitude images [Figs. 5(a), (c), and (e)]. In the case of the phase signal [Figs. 5(b), (d), (f)], the higher PTR signal belong to Cu and the lower one to steel are observed. These results reflect the fact that the thermal diffusivity is higher for Cu than steel. The PTR phase can be described using the follow equations [7]: $\phi = \frac{x}{\mu} + \phi_o$ and $\phi = x\sqrt{\frac{\pi f}{\alpha}} + \phi$. Here, $\alpha$ is the thermal diffusivity.

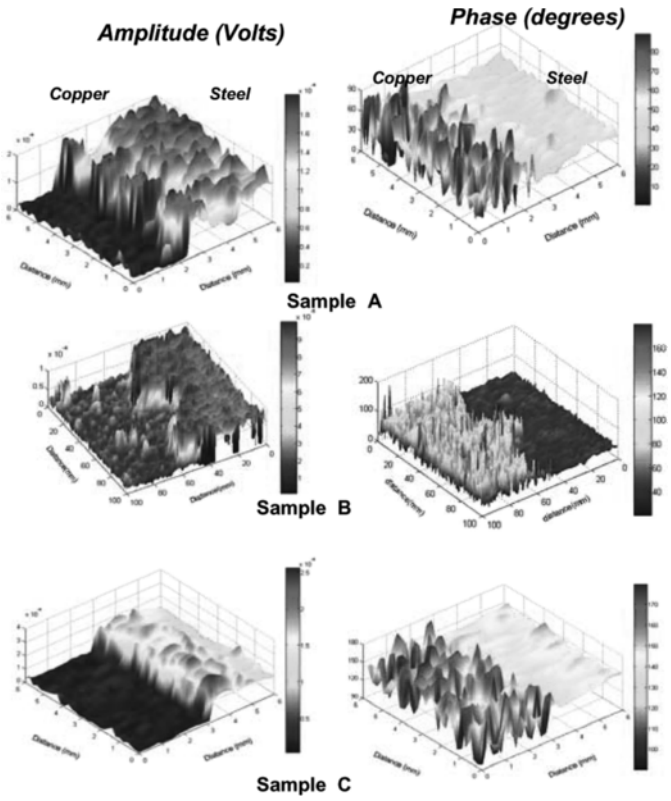


FIGURE 5.—PTR amplitude and phase images of samples A, B, and C.

According to these equations, if the thermal diffusivity coefficient is higher in Cu, this means that the PTR signal in phase should be lower than steel and that the thermal wave penetrates deeper in Cu. It is well known that the reflective and absorptive properties of materials are expressed on basis of a complex index [13]. The radiation to heat conversion in steel is greater than in Cu. Hence PTR amplitude signal of steel is bigger [Figs. 5(b), (d), and (f)]. Figure 5 shows the images of PTR on samples A, B, and C. This figure clearly demonstrates the differences in the IWZ and the IAZ on all samples resulting from the different thermal properties of Cu and steel affected by the impact.

### 3.4. XRD

The structural changes at the Cu–steel interface during the impact bonding were studied by the changes in the

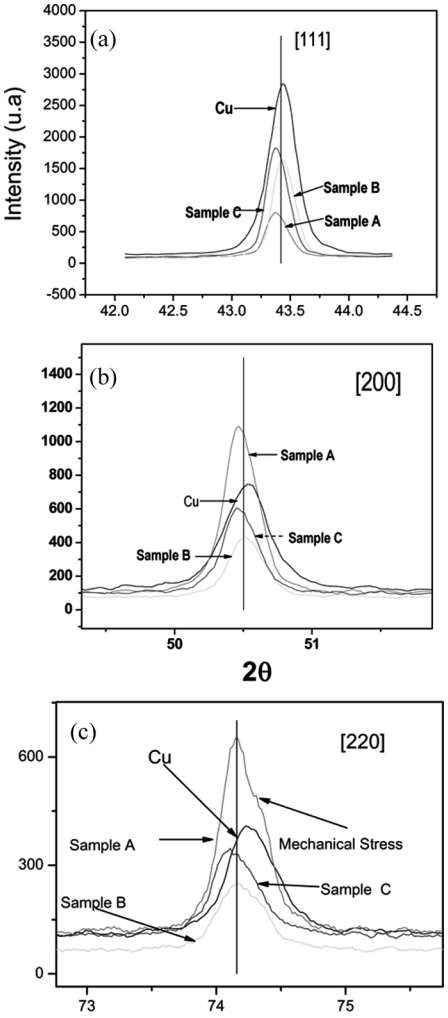


FIGURE 6.—(a), (b), and (c) show the XRD pattern of peak (111), (200), and (220) of pure Cu, as well as Cu from the impact welding region for samples A, B, and C.

crystalline quality of each metal by the changes in the FWHM of each peak and the shift thereof. Cu and steel are polycrystalline metals according to cards 04-0836 for Cu [14] and 06-0696 for Fe [15]. Figures 6(a)–(c) show the peaks (111), (200), and (220) of unbounded and bonded Cu for samples A, B, and C. The peak (111) of Cu on the three samples does not exhibit any mechanical stress.

Figures 7(a) and (b) show the XRD for (311) and (222) directions for Cu where the most dramatic changes were observed. The crystal size was modified drastically, and the crystal orientation at the welding zone almost disappears. It is well known that in this structure, a 3-1 atomic coordination exists. Further, there are also two families of planes separated by two different interplanar distances. As a result the effect of the impact process in this family of planes located at the interface is the reduction of the interplanar distance, and this produces an atomic redistribution that could generates mechanical stress.

Figures 8(a) and (b) show the (110) and (211) peak for unbounded steel, as well as those for sample A to C. The peak corresponding to steel (without impact welding)

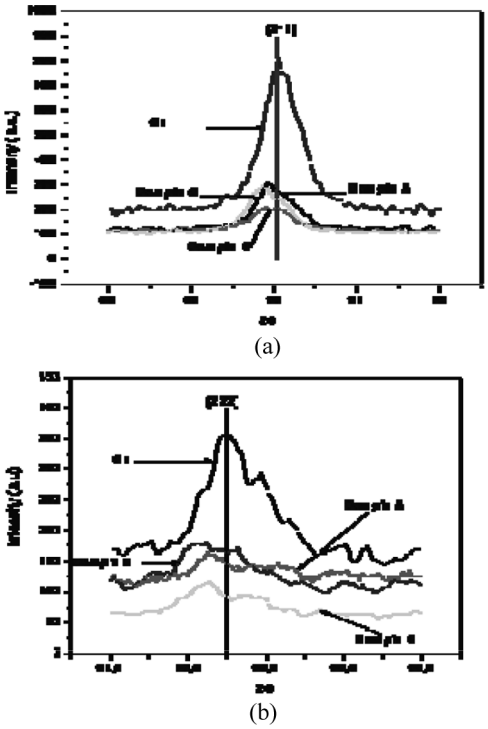


FIGURE 7.—(a) and (b) show the XRD pattern of peak (311) and (222) of Cu, for the impact welding region for samples A, B, and C.

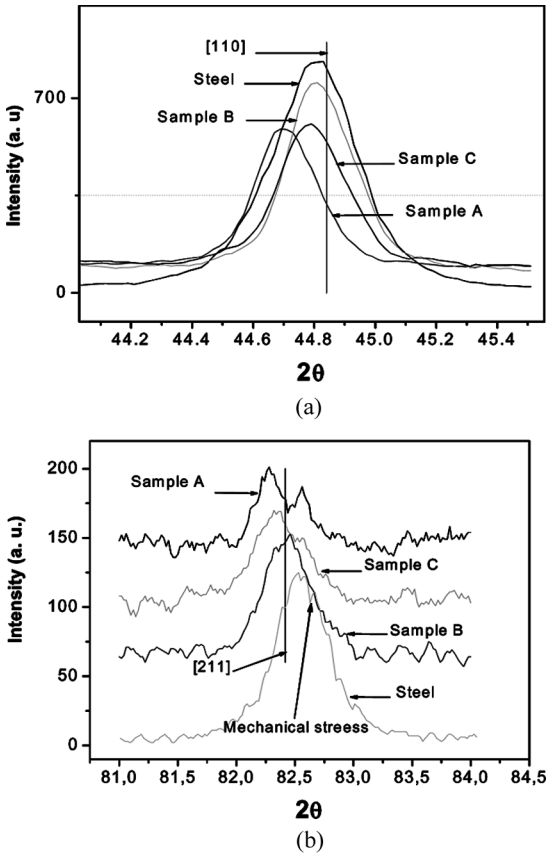


FIGURE 8.—(a) and (b) show the XRD pattern of peak (110) and (211) of steel, for the impact welding region for samples A, B, and C.

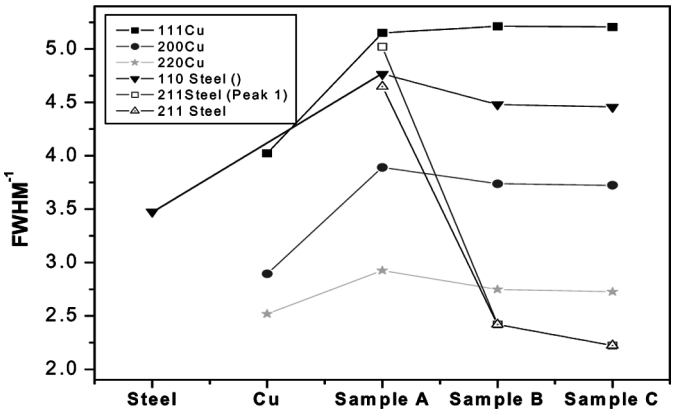


FIGURE 9.—FWHM$^{-1}$ changes of the characteristic peaks of Cu and steel.

in these directions shows mechanical stress. This stress is caused by the previous cold rolling operation on the steel plate. A noteworthy point is that in sample A and sample C is that this mechanical stress disappears after the impact bonding. In the case of (110), direction seen in Fig. 8(a), the main effect is the peak shifts to the left, this indicates an increment of lattice parameter, but without mechanical stress. An important feature in the case of (211) peak is that sample A which is the impact welding process, produces crystal with different lattice parameters. The results can be summarized by studying the changes in FWHM as crystalline quality parameter using the 1/FWHM. Low values of this parameter indicate low crystalline. Figure 9 shows the FWHM$^{-1}$ values for different peaks of Cu and steel; in the Cu lattice. The main effect after the impact is that the lattice increases its crystalline quality, while for the steel it decreases.

## 4. CONCLUSIONS

1. From Fig. 1 it is possible to define that the IWZ is formed by the collapse of grains of Cu and steel and that the IAZ is formed on both sides of the IWZ and this depends on the morphology of the impact surface; small teeth size produce a bigger effect of phase mixture and bigger IWZ.
2. Microhardness test is able to detect the IAZ but due to the dimension of the probe penetrator it is not able to detect with precision of the IWZ.
3. Noncontact PTR amplitude and phase images are able to detect the IWZ as well as the IAZ. The PTR amplitude is governed by the thermal diffusivity and effusivity, while in the case of the phase signals this is governed by the absorption coefficient. PTR is an excellent technique to characterize joined dissimilar metals and other welding methods, considering only the thermal and optical properties.
4. XRD patterns showed that after the impact no new phase is formed by Cu and steel. The results indicate that the bigger effect of the impact welding is in the Cu structure due to the lower ductility. Deformation of steel could be due to the out diffusion and redistributions of carbides which are in agreement with Rangel-Ortiz et al. [9] results as is shown in Figs. 3–5.

## ACKNOWLEDGMENTS

This work was supported by Project PAPIIT IN113606-3 2006/2009, UNAM and by the Seccion de Investigación y Posgrado del IPN, The authors wants to thanks to Ing. Q. Carmen Vazquez Ramos for sample preparation and Silvia Stroet for the technical revision of this article.

## REFERENCES

1. Gayle, F.W.; Biancaniello, F.S. Stacking Faults and Crystallite Size in Mechanically Alloyed Cu–Co, Proceedings of International Symposium on Metastable Mechanically Alloyed and Nanocrystalline Materials, 1995 edited by R. Shulz, (Trans Tech Publications, Quebec, 1995); ibid., 1996, edited by D. Fiorani and M. Magini.
2. Curiel-Reyna, E.; Herrera, A.; Castaño, V.M.; Rodríguez, M.E. Influence of cooling rate on the structure of heat affected zone alter welding a high manganese steel. Materials and Manufacturing Processes **2005**, *20*, 813–822.
3. López, G.A.; López, A.; Jaramillo, D. Estudio de la intercara de uniones entre metales disímiles por medio de ultrasonido. Rev. Metal. Madrid **1999**, *35* (1), 1–72.
4. Huang, J.Y.; Jiang, J.Z.; Yasuda, H.; Mori, H. Kinetic process of mechanical alloying in $Fe_{50}Cu_{50}$. Physical Review B **1998**-II, *58*, 817–820.
5. García, J.A.; Nicolaides, L.; Park, P.; Mandelis, A.; Farahkbahsh, B. Photothermal radiometry of thermal sprayed coatings novel roughness elimination methodology. Anal. Sci. **2001**, *17*, 89–92.
6. Velázquez-Hernández, R.; García-Rivera, J.; Jiménez-Sandoval, S.; Mendoza-Álvarez, J.G.; Garcia, J.A.; Rodríguez, M.E. Photothermal, photocarrier and Raman characterization of Te doped GaSb. J. Appl. Phys. **2007**, *101*, 023105–023108.
7. Garcia, J.A.; Mandelis, A.; Farahbakhsh, B.; Lebowits, C.; Harris, I. Thermophysical properties of thermal sprayed coatings on carbon steel substrates by photothermal radiometry. Inter. J. Thermophysics **1999**, *20* (5), 1587–1602.
8. Rodríguez, M.E.; Mandelis, A.; Pan, G.; García, J.A.; Riopel, Y. Microelectronic circuit characterization via photothermal radiometric of Scribe lines recombination lifetime. Solid-State Electron **2000**, *44*, 703–711.
9. Rangel-Ortiz, T.; Chávez-Alcalá, F.; Curiel-Reyna, E.; Del Real, A.; Baños, L.; López-Hirata, J.; Rodríguez-García, M.E. Structural and mechanical characterization of As-Cast Al–Li–Hf alloy. Materials and Manufacturing Processes **2007**, *22*, 1–5.
10. Liu, Y.; Baddour, N.; Mandelis, A. Transverse depth-profilometric hardness photothermal phase imaging of heat treated steels. J. Appl. Phys. **2003**, *94*, 5543–5548.
11. Mandelis, A. Laser infrared photothermal radiometry of semiconductors: principles and application to solid state electronics. Solid-State Electron **1998**, *42*, 1–15.
12. Touloukian, Y.S.; Powell, R.W.; Ho, C.Y.; Nicolaou, M.C. *Thermophysical Properties of Matter 10*. Thermal Diffusivity. TFT Plenum: New York, Washington, 1973; p. 51.
13. Palik, E.D. *Handbook of Optical Constants of Solids I and II*; Academic Press: London, 1985.
14. Swanson, H.E. US Natl Bur. Stand. 1953, Circular No. 539, I.15.
15. Swanson, H.E.; Gilfrich, T.; Ugrinie, M. US Natl Bur. Stand 1955, Circular No. 539, IV.3.